Open Access Online Journal on Astronomy and Astrophysics

Acta Astrophysica Taurica

www.astrophysicatauricum.org

Acta Astrophys. Tau. 7(1), 4–7 (2026) EDN: TVQWNZ

Compensation for low-frequency and quasistatic aberrations in stellar spectroscopy

E.V. Emelianov, M.V. Yushkin, Yu.B. Verich, V.E. Panchuk

Special Astrophysical Observatory of the Russian Academy of Sciences, Nizhnij Arkhyz 369167, Zelenchukskiy region, Karachai-Cherkessian Republic, Russia
e-mail: eddy@sao.ru

Received 9 December 2023

ABSTRACT

We report methods for correcting low-frequency variations in the position of the star image at the input of the spectral equipment at the BTA Nasmyth and primary foci, used for the past two decades at the telescope. New technical solutions make it possible to extend the operating frequency range to 6 Hz for stars brighter than 10^m.

Key words: spectral instrumentation, aberration correction

1 Introduction

Since 2000, a local wavefront tilt corrector (LTC, Ivanov et al., 2001) has been operating at the Nasmyth focus of the 6-m BTA telescope, which facilitates the work of the observer and provides gain in throughput by one magnitude on the Nasmyth Echelle Spectrograph (NES; Panchuk et al., 2017) and the Main Stellar Spectrograph (MSS; Panchuk et al., 2014). Accounting for the extensive operational experience in using this system, the development of a new local corrector of the BTA Nasmyth focus was initiated in 2020. Thus, the rich statistics of the LTC operation are taken into account, which allowed, in particular, the detection of the anisotropy of image oscillations caused by wind load on the telescope structure (Tamarov et al., 2022).

The sources of low-frequency image oscillations are:

- wind load on the telescope tube,
- imperfections of the control system,
- air masses near the dome shutter,
- atmospheric density waves,
- oscillations of the BTA main mirror in its cell,
- temperature variations of the telescope components and the main mirror.

In addition to objective statistics, the staff of the Laboratory of Astrospectroscopy[1] have accumulated subjective experience over decades of observations at the BTA. In particular, it is known that the characteristics of fluctuations in the position of images are not necessarily related to fluctuations in their shape (sometimes the diameter of a stably positioned image changes noticeably, up to separation of the whole into fragments). In other words, even in good images, low-frequency correction of wavefront tilts is necessary.

2 Characteristics of low-frequency image oscillations

Klochkova et al. (2020) noted the prevailing frequencies of image oscillations identified over the years of operation of the BTA: in the $0.7 \div 0.9$ Hz range along both axes, as well as in the $0.8 \div 1$ Hz range for the azimuth axis and 0.4 Hz for the zenith distance axis. When correcting the position of an object through the influence on the telescope drives, oscillations arise with a decay time of about 25 s. In May 2023, after installation of new frequency converters of the BTA axis motors, studies on the accuracy of object tracking were carried out again. For this purpose, several series of images of bright stars were obtained with short exposures ($50 \div 200$ ms, with the accuracy of calculating the centroid of $0.''05$). Frequency analysis revealed the presence of several vibration harmonics.

Figure 1 presents a plot of oscillations of the Polaris image at the BTA primary focus. In the low-frequency region of the oscillation spectrum, two peaks are evident: near $0.7 \div 0.8$ Hz (for both axes) and near 0.9 Hz (more prominent for the zenith axis). Lower-frequency oscillations are buried in noise, indicating their aperiodic nature. These two peaks are inherent to the telescope mechanics, since when all control systems are completely disabled (including the hydrostatic bearing oil supply), the image oscillation spectrum relative to the natural trend line exhibits no periodic structures, displaying a purely aperiodic character.

Even slower are the image oscillations caused by the displacement of the main mirror (MM) in its cell. The top panel

[1] https://www.sao.ru/hq/ssl/

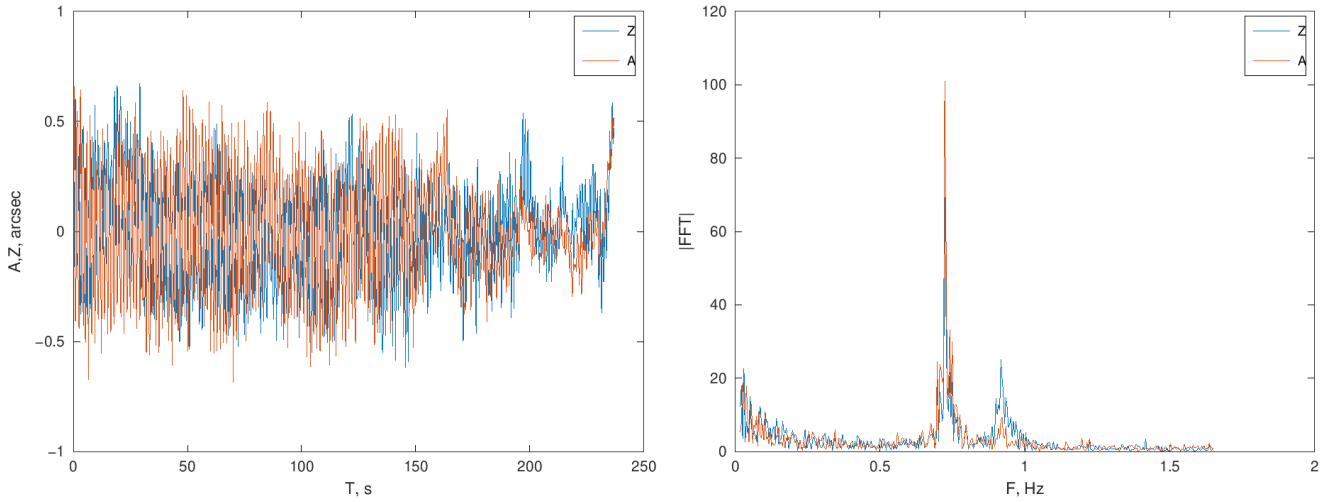

Fig. 1. Star image oscillations at the BTA primary focus (left) and the oscillation spectrum (right).

of Fig. 2 shows the detected oscillations of the main mirror within its cell. The largest amplitude is reached by oscillations causing image displacement along the azimuthal axis (about 8″ over the entire working range of zenith distances, which corresponds to an image shift of 16″). The plot reveals the presence of hysteresis in these oscillations. The bottom panel of the figure shows the hysteresis plot (the difference between the upper and lower curves), which reaches a maximum of about 3.″5, i.e., when pointing the telescope to an object using the averaged coefficients of the pointing correction system (PCS), the deviation of the object position from the computed one due to hysteresis can amount to 3.″5. These oscillations arise due to the changes in the tilt of the telescope tube along the Z axis and accordingly have periods of tens of minutes or even hours.

Even slower are the aberrations caused by temperature inhomogeneity of the main mirror. In 2018, 80 temperature sensors were installed on the MM of the BTA (60 in the recesses beneath the mirror support and 20 on the rear surface). It was established that the temperature gradient can give rise to both defocus and astigmatism (as well as some other aberrations). Due to the large thermal inertia of the MM (Emelianov, 2015), the period of these oscillations is of the order of one day. However, it is known that defocus also arises from temperature changes in the telescope tube struts, and these changes produce noticeable effects on timescales of tens of minutes to a few hours.

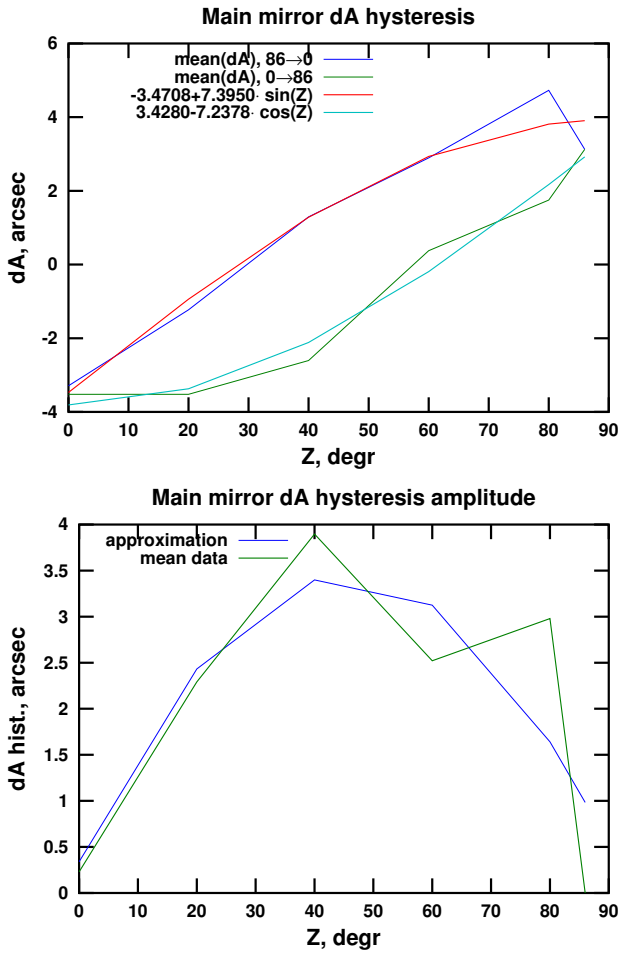

Fig. 2. Hysteresis of the main mirror oscillations.

3 Hardware solutions

In the aforementioned LTC, the key element is a plane-parallel quartz plate whose tilts provide the required wavefront tilt. The coordinates are determined from the wings of the star image on the slit jaws using a TV viewer. The relative aperture of $f/30.7$ allows the plane-parallel plate to operate with almost no introduced aberrations.

During the development of the primary focus spectrograph ESPriF, the relative aperture of $f/4$ and the mass and size constraints on the primary focus hardware required to replace the plane-parallel plate with a movable lens. This unit turned out to be universal: it can operate with both the slit

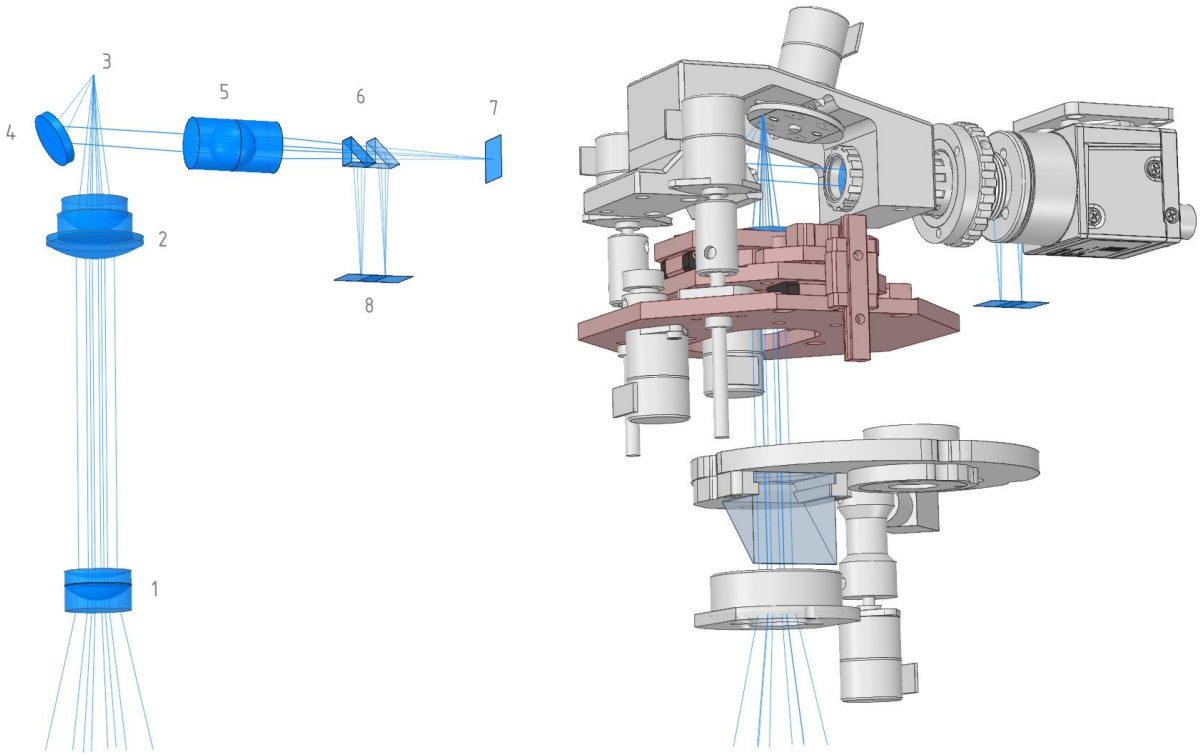

Fig. 3. Pre-slit part of ESPriF. Designations: left – ray path, right – principal elements and units. 1 and 2 – elements of the afocal reducer, 3 – slit (decker) position, 4 and 5 – decker viewer optics, 6 – beam-splitting elements of the defocus detector, 7 and 8 – decker viewer detectors.

and fiber-optic inputs. Furthermore, by replacing the collimator unit at the device input, there appears a possibility to use such a device on smaller telescopes, for example, on the Zeiss-1000 telescope with a relative aperture of $f/13$.

An optical design of the new ESPriF pre-slit part was implemented (see Fig. 3), comprising the following elements:

1. Afocal reducer – a lens system converting the converging beam of rays from the main mirror of the BTA into a converging beam with the same relative aperture, but with the ability of quick defocusing compensation by shifting one optical element. The same movable element also provides wavefront tilt compensation by moving along two orthogonal axes in a plane perpendicular to the principal axis of the reducer.
2. Entrance slit viewer with a defocus detector – a projection lens with beam-splitting cubes in a converging beam.
3. Polarimetric module including two superachromatic phase-shifting plates – a quarter-wave and a half-wave plate, as well as a Savart plate with the ability of inserting the latter behind the entrance slit of the spectrograph with simultaneous compensation of defocus by shifting the collimator.
4. Calibration channel.

In the left panel of Fig. 3, the principal optical elements of the input module of the hanging spectrograph are indicated. In the case of slit input, elements 6 and 8 are absent. For fiber-optic input, mirror 4 is replaced by a beam-splitting cube that diverts up to 10 % of the light into the viewer channel, and detector 7 is moved to position 8, simultaneously providing control of both defocus and image displacement.

In addition to the three-axis stage and the slit turret, the input unit contains nodes for inserting and removing calibration and polarization optics. All these elements are driven by miniature stepper motors. A universal controller for eight independent stepper motors[2] was developed to control the movable elements of the input unit, connected to the computer via USB or CAN interfaces.

The core of the control system is a mini-computer running Calculate Linux, located directly within the hanging part of the spectrograph. The unified instrument control interface is a graphical shell (web interface) for several system daemons: obtaining scientific images, obtaining images from the slit/deckers viewing camera, controlling the spectrograph nodes, and controlling the low-frequency wavefront corrector.

Obtaining images from the viewing camera is an independent operation. The last obtained image is contained in a buffer, which can be transmitted to any client upon a network request: for visual display or for calculating the coordinates of the star centroid. In automatic correction mode, a separate application – the corrector daemon – controls the gain level and exposure of the CMOS detector and sets the region of interest (to increase the speed of readout and data transfer). The region of interest typically coincides with the limiting zone in which autocorrection by mechanical movements of

[2] https://github.com/eddyem/stm32samples/tree/master/F3:F303/Multistepper

the lens unit is available. After calculating the centroid coordinates, the required value of lens displacement is determined to compensate for the corresponding wavefront tilt. This value is calculated by a software PID controller. When the corrector lens reaches the limit of movement, the telescope drives are commanded (in correction mode) to move the current image position to the center of the permissible area of lens movement. The decaying oscillations of the image that arise as a result of the telescope movement are then compensated by displacements of the lens corrector.

4 Conclusions

Experience in the development and operation of low-frequency star image correctors at relative apertures of $f/30$ (Nasmyth focus of the BTA) and $f/13$ (1-meter telescope) made it possible to build a corrector for the tilt and curvature of the wavefront for the primary focus of the BTA ($f/4$). Tests of the corrector at the telescope confirmed the correctness of the basic technical solutions. The inertia of mechanical drives, which determines the limit of correction frequencies at the Nasmyth-2 focus, has been structurally overcome in the new device. Numerical estimates have shown that for most objects whose spectroscopy requires image correction, the upper frequency limit is determined not by the mechanical properties of the corrector, but by the sensitivity of the object registration system and the features of the algorithm for generating executive commands. We plan to use the found technical solutions on other spectral devices.

Acknowledgments. Observations at the 6-meter telescope of the SAO RAS are supported by the Ministry of Science and Higher Education of the Russian Federation. Financial support was provided by grant No. 075-15-2022-262 “Multi-wavelength study of nonstationary processes in the Universe” (13.MNPMU.21.0003).

References

Emelianov E.V., 2015. Astrophys. Bull., vol. 70, iss. 3, pp. 362–370.

Ivanov A.A., Panchuk V.E., Shergin V.S., 2001. SAO RAS preprint No 155, pp. 1–19. (In Russ.)

Klochkova V.G., Sheldakova Yu.V., Vlasyuk V.V., Kudryashov A.V., 2020. Astrophys. Bull., vol. 75, iss. 4, pp. 468–481.

Panchuk V.E., Chuntonov G.A., Naidenov I.D., 2014. Astrophys. Bull., vol. 6, iss. 3, pp. 339–355.

Panchuk V.E., Klochkova V.G., Yushkin M.V., 2017. Astron. Rep., vol. 61, iss. 9, pp. 820–831.

Tamarov V.A., Tavolzhanskaya A.S., Panchuk V.E., 2022. XI All-Russian conference “System synthesis and applied synergetics”. Rostov-on-Don – Taganrog: South Federal University Publishing House, pp. 279–281. (In Russ.)